Measurement of transparent plates with wavelength-tuned phase-shifting interferometry

Peter de Groot

A wavelength-tuned Fizeau interferometer is applied to the problem of flatness testing of transparent plates. When the plate is positioned at a specific distance from the reference surface and an integer-math 13-frame phase-shifting algorithm is applied, the system directly filters out unwanted interference arising from backsurface reflections. The resulting front-surface profile exhibits less than 2 nm of residual error attributable to spurious reflections from within the plate. © 2000 Optical Society of America

OCIS codes: 120.3180, 120.3940, 120.5050, 120.5060, 120.6650, 220.4840.

1. Introduction

A common problem in optical surface profiling is spurious reflections, such as are encountered when the flatness of a transparent plate is tested in a Fizeau interferometer.[1] Unwanted interference effects arising from backsurface reflections result in the complex mixture of fringes shown in Fig. 1. The overlapping patterns render ineffective standard techniques in phase-shifting interferometry (PSI), which rely on the analysis of a sequence of interference images shifted in phase by mechanical modulation of the reference flat. Common practice is to defeat backsurface reflections by one applying an index-matching coating and then proceeding with standard PSI. It would be desirable to dispense with such surface treatments for routine inspection of transparent plates, particularly for process control in a production environment.

Several alternatives are now available, including white light,[2] grazing incidence,[3] desensitized grating interferometry,[4] use of multimode laser diodes,[5] and combinations of measurements in different orientations.[6] An important class of solutions involves tunable-wavelength sources. Okada *et al.*, for example, have measured transparent plates in a Twyman–Green interferometer by acquiring 60 interference images at a sequence of wavelengths and least-squares fitting of the first-order terms to calculate surface and optical thickness profiles.[7,8]

Here I propose to measure transparent plates by using a wavelength-tuned laser Fizeau interferometer and a PSI algorithm that directly suppresses interference modulations that are attributable to spurious reflections (patent pending). The resulting phase map represents only the desired front-surface reflection and is relatively free of distortions, in spite of the complex nature of the interference pattern. Apart from use of a wavelength-tunable source and the need to position the object rather closely to the reference flat, the technique involves few changes to a standard laser-based Fizeau. The PSI algorithm executes quickly for high-throughput production testing. The approach should prove useful to qualify optical components, flat panel displays, and transparent substrates for rigid disk drives.

2. Interferometry of Transparent Plates

Figure 2 shows the optical geometry leading to the interference pattern shown in Fig. 1. The phase delay from the reference surface to the front object surface is

$$\theta = 2k(h_1 - h_0) + 2kL, \tag{1}$$

where L is the nominal distance to the front object surface and the angular wave number k is 2π divided by the wavelength λ. The phase delay from the front to the back object surfaces is

$$\phi = 2kn(h_2 - h_1) + 2knT, \tag{2}$$

P. de Groot (peterd@zygo.com) is with the Department of Research and Development, Zygo Corporation, 21 Laurel Brook Road, Middlefield, Connecticut 06455-0448.

Received 28 October 1999; revised manuscript received 16 February 2000.

0003-6935/00/162658-06$15.00/0

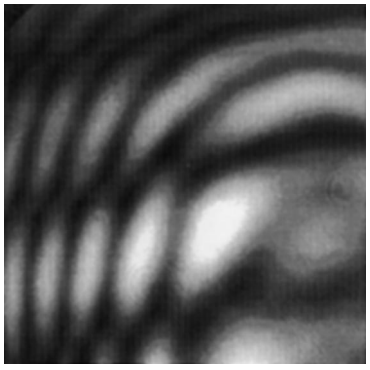

Fig. 1. Fringe pattern in a Fizeau interferometer when viewing a transparent plate. The complicated interference effects, including backsurface reflections, defeat conventional PSI with mechanical phase shifting.

where nT is the nominal optical thickness of the transparent plate object. In Eqs. (1) and (2), $h_{0,1,2}$ are the height profiles for the reference front object and back object surfaces, respectively, and $r_{0,1,2}$ are the corresponding amplitude reflectivities.

In the absence of the backsurface reflection, PSI would provide the phase difference θ given by Eq. (1) to an arbitrary integer multiple of 2π, which together with knowledge of the reference surface h_0 and the wave number k provides a relative surface profile proportional to h_1. In the more general situation, the interference intensity is

$$g = |u|^2, \tag{3}$$

where

$$u = \frac{r_0 + r' \exp(i\theta)}{1 + r' r_0 \exp(i\theta)}, \tag{4}$$

$$r' = \frac{r_1 + r_2 \exp(i\phi)}{1 + r_1 r_2 \exp(i\phi)}. \tag{5}$$

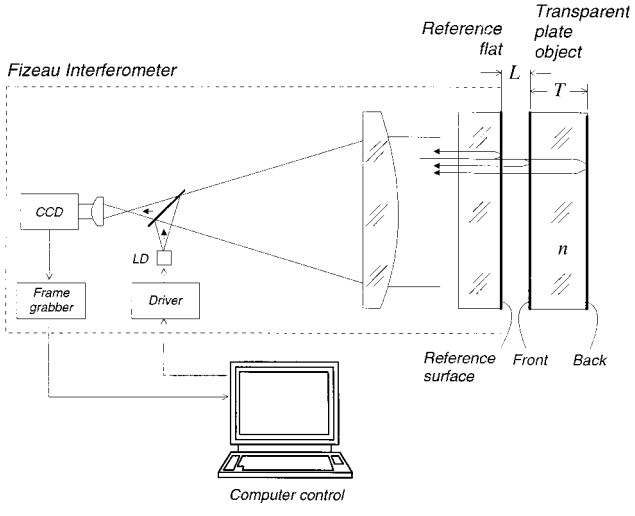

Fig. 2. Laser-based Fizeau interferometer viewing a transparent plate. LD, laser diode.

This calculation includes all possible multiple reflections between the reference surface and the two surfaces of the transparent plate. A simplified example calculation assumes here that the intensity reflectivity R is identical for all three surfaces:

$$\begin{aligned} r_0 &= -\sqrt{R}, \\ r_1 &= \sqrt{R}, \\ r_2 &= -\sqrt{R}. \end{aligned} \tag{6}$$

Using this simplifying assumption and expanding Eqs. (3)–(5), I find that for this example

$$g = 2R\left[\frac{3}{2} - \cos(\theta) - \cos(\phi) + \cos(\theta + \phi)\right] + O(R^2). \tag{7}$$

The first-order terms in R already reveal the difficulty of performing PSI on transparent plates. Terms involving the phase ϕ introduce an unwanted dependence of the interference data on the height profile h_2 of the backsurface of the transparent plate. Standard PSI, which relies on a mechanical modulation of θ, is unable to make sense of the resulting interference behavior.

3. Wavelength-Tuned Phase-Shifting Interferometry

Controlled wavelength tuning—for example, by injection current modulation of a laser diode in an unequal-path interferometer—is a convenient nonmechanical means of generating phase shifts for PSI.[9,10] Wavelength-tuned PSI has a further advantage in dealing with overlapping interference patterns from multiple reflections. As the wave number ramps with time at a rate dk/dt, the interference intensity varies according to

$$g(t) = 2R\left[\frac{3}{2} - \cos(\theta + \nu_1 t) - \cos(\phi + \nu_2 t) + \cos(\theta + \phi + \nu_3 t)\right] + O(R^2), \tag{8}$$

where

$$\nu_1 = 2L\,dk/dt, \tag{9}$$

$$\nu_2 = \Gamma\nu_1, \tag{10}$$

$$\nu_3 = (\Gamma + 1)\nu_1, \tag{11}$$

$$\Gamma = nT/L. \tag{12}$$

Wavelength tuning modulates the various terms in Eq. (8) at different rates, therefore providing a means in principle of one distinguishing between their contributions to the final interference image.

Table 1 summarizes the modulation frequencies $\nu_{1\ldots3}$ and $\nu_{4\ldots9}$ for first- and second-order terms of Eq. (8), respectively. For example, $\Gamma = 3$ might involve a $T = 12$-mm-thick transparent glass plate of index $n = 1.5$ placed at a distance $L = 6$ mm from the reference surface. The resulting interference mod-

Table 1. Modulation Frequencies Resulting from Wavelength Tuning a Fizeau Interferometer with a Transparent Plate Object[a]

Modulation Frequency	Frequency $2Ldk/dt$	$\Gamma = 3$	$\Gamma = 0.5$	Amplitude $2R(1 - 4R)$
ν_1	1	1	1	-1
ν_2	Γ	3	0.5	-1
ν_3	$\Gamma + 1$	4	1.5	1
ν_4	2	2	2	$-R$
ν_5	$\Gamma - 1$	2	-0.5	$-R$
ν_6	$\Gamma + 2$	5	2.5	$2R$
ν_7	2Γ	6	1	$-R$
ν_8	$2\Gamma + 1$	7	2	$2R$
ν_9	$2\Gamma + 2$	8	3	$-R$

[a] $\Gamma = nT/L$.

ulations include the fundamental frequency ν_1 for the front-surface reflection, plus the spurious harmonics $\nu_{2\ldots9}$ listed in Table 1 and shown graphically in Figs. 3 and 4. Although these unwanted modulations confuse conventional PSI, it should be possible in principle to identify and suppress these terms according to their modulation frequency.

4. Fourier Filtering with Phase-Shifting Algorithms

Phase-shifting algorithms are essentially single-frequency Fourier transforms tuned to the expected interference modulation frequency ν_1. Consequently, all PSI algorithms have, to some degree, the ability to suppress signal distortions at other frequencies.[11] I therefore propose to construct an efficient integer-math PSI agorithm that is specifically designed to extract the desired front-surface interference information while directly filtering out the unwanted modulation frequencies $\nu_{2\ldots9}$.

Not all PSI algorithms are appropriate to this task, so the first step is to identify an algorithm having the

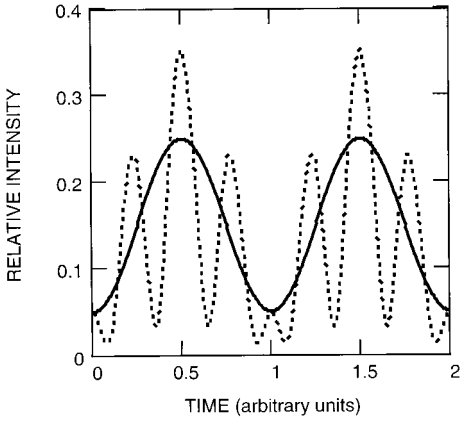

Fig. 3. Single-pixel intensity modulation in a Fizeau interferometer during a continuous shift in source wavelength. The solid curve represents the expected signal from a single object surface. The dotted curve represents the signal when viewing a transparent plate object, including unwanted distortions resulting from spurious backsurface reflections.

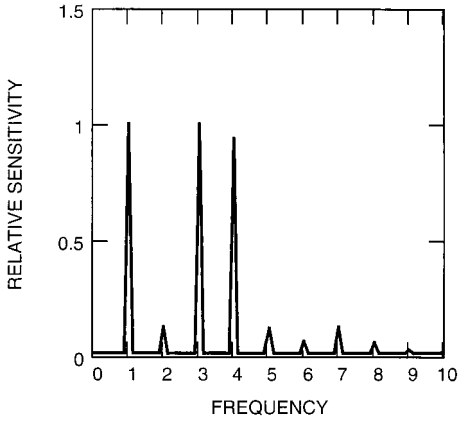

Fig. 4. Frequency content of the dotted-curve signal shown in Fig. 3. The desired fundamental frequency ν_1, here normalized to 1, is accompanied by several parasitic modulations as noted in Table 1.

desired filtering characteristics. Most PSI algorithms can be written as follows:

$$\theta = \tan^{-1}\left(\sum_{m=0}^{M-1} s_m g_m \Big/ \sum_{m=0}^{M-1} c_m g_m\right) + \text{const}, \quad (13)$$

where the index m corresponds to successive camera frames and s_m and c_m are coefficients specific to the PSI algorithm. The total number of frames M is typically between 4 and 7. The interference phase shifts continuously between camera frames by an amount

$$\Delta\alpha = \nu_1 \Delta t, \quad (14)$$

where Δt is the time lapse between frames. PSI algorithms are designed to be sensitive to this phase shift and to be resistant to distortions in the phase shift as well as other disturbances.

One way to evaluate the sensitivity of PSI algorithms to unwanted interference terms is to perform a discrete Fourier transform of the coefficients s_m and c_m:

$$S(\nu) = \sum_{m=0}^{M-1} s_m \exp(-im\Delta\alpha\nu/\nu_1), \quad (15)$$

$$C(\nu) = \sum_{m=0}^{M-1} c_m \exp(-im\Delta\alpha\nu/\nu_1). \quad (16)$$

The resulting filter functions $S(\nu)$ and $C(\nu)$ are transfer functions in the frequency domain.[12] A measure of the characteristic sensitivity of the algorithm to intensity noise is therefore

$$I(\nu) = [|S(\nu)|^2 + |C(\nu)|^2]^{1/2}. \quad (17)$$

Perhaps the best way to illustrate use of the filter function analysis is to give an example of what will not work in the present application. The most commonly used PSI algorithm today is the Schwider–

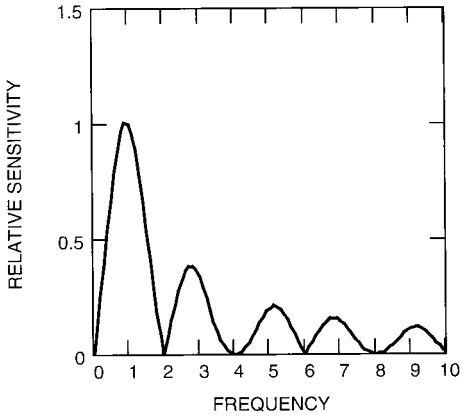

Fig. 5. Theoretical frequency response of the five-frame, $\Delta\alpha = \pi/2$ PSI algorithm, including the averaging or integrating bucket effect of the phase change during the data-acquisition time interval Δt. Unfortunately this algorithm is sensitive to the unwanted harmonics shown in Fig. 4.

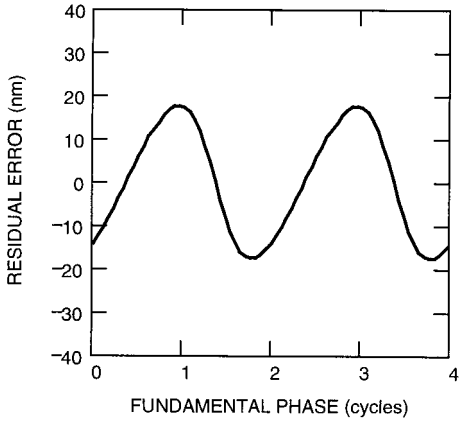

Fig. 6. Theoretical cyclic error as a function of the fundamental phase θ for a five-frame PSI algorithm in the presence of reflections.

Hariharan five-frame algorithm,[1,13] for which the coefficients are

$$s = (0 \quad 2 \quad 0 \quad -2 \quad 0), \tag{18}$$

$$c = (-1 \quad 0 \quad 2 \quad 0 \quad -1). \tag{19}$$

The filter functions are

$$S(\nu) = i \sin(\pi\nu/2\nu_1), \tag{20}$$

$$C(\nu) = \sin^2(\pi\nu/2\nu_1). \tag{21}$$

The algorithm has periodic extrema at $\nu/\nu_1 = 1, 3, 5 \ldots$, meaning that it is sensitive to modulations at these frequencies. Figure 5 shows this sensitivity graphically by use of Eqs. (17), (20), and (21). For the $\Gamma = 3$ example in Table 1, the ν_2 modulation overlaps the $\nu/\nu_1 = 3$ sensitivity and is therefore unfiltered by the five-frame PSI algorithm. The amplitude of this unwanted ν_2 modulation is the same as the fundamental and is fatal to PSI for this value of Γ, as is clear from the ± 20-nm cyclic errors plotted in Fig. 6. There does not appear to be a value of Γ that would make it possible to place the first-order ν_2 and ν_3 frequencies simultaneously at the zeros of Eqs. (20) and (21).

A PSI algorithm that is better suited to the task of filtering unwanted interference modulations in transparent plates is the following 13-frame, $\Delta\alpha = \pi/4$ algorithm[14,15]:

$$s = (-3 \quad -4 \quad 0 \quad 12 \quad 21 \quad 16 \quad 0 \quad -16 \quad -21 \quad -12 \quad 0 \quad 4 \quad 3), \tag{22}$$

$$c = (0 \quad -4 \quad -12 \quad -12 \quad 0 \quad 16 \quad 24 \quad 16 \quad 0 \quad -12 \quad -12 \quad -4 \quad 0). \tag{23}$$

The filter functions in Fig. 7 show that the 13-frame algorithm suppresses both the first-order harmonics $\nu_{2,3}$ for the $\Gamma = 3$ example in Table 1, as well as most of the second-order terms. The residual error that is attributable to the $\nu_8/\nu_1 = 7$ modulation is ± 2 nm. Thus the 13-frame PSI algorithm combined with the transparent plate being placed close to the reference surface nearly eliminates the effect of backsurface reflections.

There are several other system configurations and algorithms that use the same principle. An interesting alternative is the case in which $\Gamma = 0.5$. The two first-order unwanted modulations according to Table 1 are now at $\nu_2/\nu_1 = 0.5$ and $\nu_3/\nu_1 = 1.5$. The sensitivity curve in Fig. 8 shows how the following 15-frame, $\Delta\alpha = \pi/2$ algorithm suppresses these unwanted modulations:

$$s = (-1 \quad 0 \quad 9 \quad 0 \quad -21 \quad 0 \quad 29 \quad 0 \quad -29 \quad 0 \quad 21 \quad 0 \quad -9 \quad 0 \quad 1), \tag{24}$$

$$c = (0 \quad -4 \quad 0 \quad 15 \quad 0 \quad -26 \quad 0 \quad 30 \quad 0 \quad -26 \quad 0 \quad 15 \quad 0 \quad -4 \quad 0). \tag{25}$$

The second-order ν_7 and ν_9 terms result in a residual error of ± 2 nm. The $\Gamma = 0.5$ case positions the part

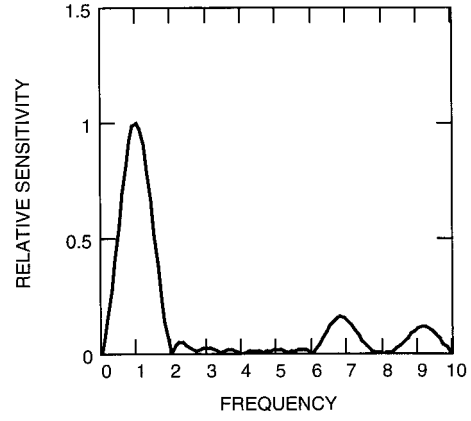

Fig. 7. Theoretical frequency response of the 13-frame, $\Delta\alpha = \pi/4$ PSI algorithm. This algorithm suppresses the high-frequency modulations shown in Figs. 3 and 5.

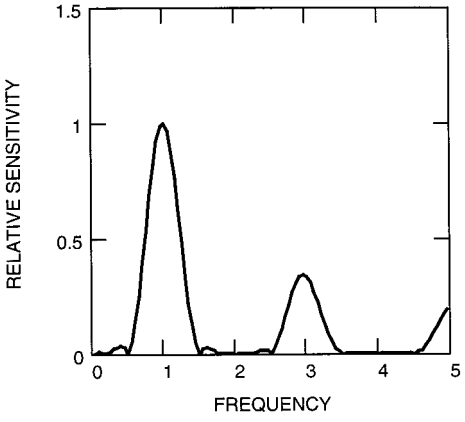

Fig. 8. Theoretical frequency response of the 15-frame, $\Delta\alpha = \pi/2$ PSI algorithm. This algorithm is effective at suppressing spurious modulations for the case in which $\Gamma = 0.5$ (see Table 1). Note the change in horizontal scale with respect to Figs. 6 and 7.

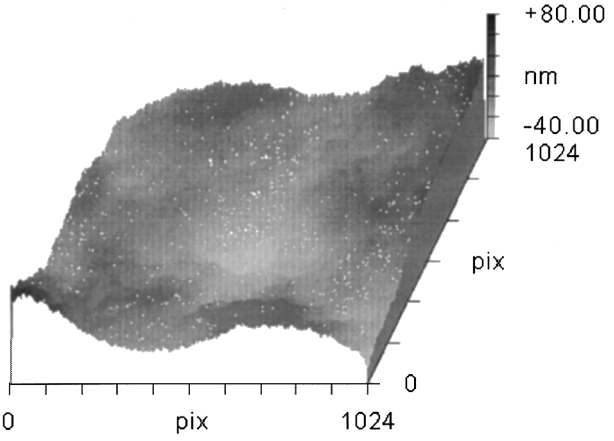

Fig. 10. Experimental data showing the suppression of profile distortions when wavelength-tuned interferometry is used with the 13-frame, $\Delta\alpha = \pi/4$ PSI algorithm described in the text. The transparent plate object is identical to the one profiled in Fig. 9.

at a more comfortable distance than the $\Gamma = 3$ example, i.e., six times further away. The relative advantage of the $\Gamma = 3$ solution is that it tolerates a large variation in object position, and it actually works well with values of Γ ranging from 2 to 5. The $\Gamma = 0.5$ solution requires the object to be positioned at the precise distance L to within a few percent, and likewise it requires a more precise calibration of the wavelength excursion.

5. Experiment

The technique was evaluated for the inspection of 10-cm-thick, 0.6-m-diameter transparent flats generated by large rotational polishing machines. The object placement distance is $L = 5$ cm for $\Gamma = 3$. Figure 1 shows a single frame of the interference intensity data for this object. The large-aperture interferometer uses a wavelength-tunable laser diode source.[16]

Figure 9 shows the results of a first experiment with a conventional five-frame PSI analysis, for which the high-frequency profile distortions are attributable to the backsurface reflection. Figure 10 shows the results of a second experiment, in which the 13-frame PSI algorithm together with wavelength tuning eliminates the distortion. For this latter experiment, the angular wave-number excursion Δk per camera frame is 0.079 cm^{-1}. The total wavelength excursion for a nominal wavelength λ of 0.68 μm is 0.0075 nm. The residual error is undetectable, consistent with the predicted improvement.

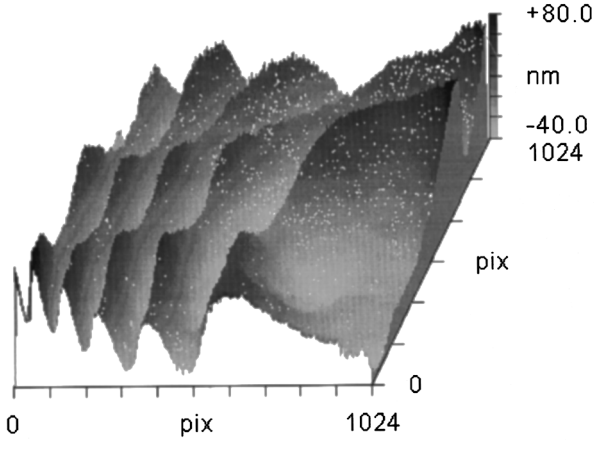

Fig. 9. Experimental data processed with the five-frame, $\Delta\alpha = \pi/2$ PSI algorithm showing the predicted 40-nm peak-to-valley profile distortion resulting from backsurface reflections from a transparent plate.

6. Conclusions

The foregoing experimental demonstration verifies one possible combination of part placement with a PSI algorithm that suppresses unwanted modulations in the interference intensity. There are many other possible combinations that rely on the same principle. The key is to match the modulation frequencies determined by expansion of Eqs. (3)–(5) with the PSI algorithm sensitivity determined by Eq. (17). In many cases, this will require construction of a new PSI algorithm by use of any one of the known techniques.[17,18] Once this is accomplished, it is possible to profile accurately transparent plates with laser-based Fizeau interferometry.

This research was initiated by T. Connolly and was completed with the able assistance of J. Soobitsky, who performed the experiments with the Zygo 24-in. phase-shifting interferometer.

References and Notes

1. J. Schwider, R. Burow, K.-E. Elssner, J. Grzanna, R. Spolaczyk, and K. Merkel, "Digital wave front measuring interferometry: some systematic error sources," Appl. Opt. **22,** 3421–3432 (1983).
2. K. Freischlad, "Large flat panel profiler," in *Flatness, Roughness, and Discrete Defect Characterization for Computer Disks, Wafers, and Flat Panel Displays*, J. C. Stover; ed. Proc. SPIE **2862,** 163–171 (1996).
3. P. G. Dewa and A. W. Kulawiec, "Grazing incidence inter-

ferometry for measuring transparent plane-parallel plates," U.S. patent 5,923,425 (13 July 1999).
4. P. de Groot, "Grating interferometer for metrology of transparent flats," in *Optical Fabrication and Testing*, Vol. 6 of 1996 OSA Technical Digest Series (Optical Society of America, Washington, D.C., 1996), pp. 28–30.
5. C. Ai, "Multimode-laser interferometric apparatus for elimination background interference fringes from thin-plate measurements," U.S. patent 5,452,088 (19 September 1995).
6. P. de Groot, "Metrology of transparent flats," in *Optical Fabrication and Testing Workshop*, Vol. 13 of 1994 OSA Technical Digest Series (Optical Society of America, Washington, D.C., 1994), pp. 160–168.
7. K. Okada and J. Tsujiuchi, "Wavelength scanning interferometry for the measurement of both surface shapes and refractive index inhomogeneity," in *Laser Interferometry: Quantitative Analysis of Interferograms*, R. J. Pryputniewicz, ed., Proc. SPIE **1162,** 395–401 (1989).
8. K. Okada, H. Sakuta, T. Ose, and J. Tsujiuchi, "Separate measurements of surface shapes and refractive index inhomogeneity of an optical element using tunable-source phase shifting interferometry," Appl. Opt. **29,** 3280–3285 (1990).
9. G. E. Sommargren, "Interferometric wavefront measurement," U.S. patent 4,594,003 (10 June 1986).
10. P. S. Fairman, B. K. Ward, B. F. Oreb, and D. I. Farrant, "300-mm aperture phase shifting Fizeau interferometer," Opt. Eng. **38,** 1371–1380 (1999).
11. K. G. Larkin and B. F. Oreb, "Design and assessment of symmetrical phase-shifting algorithms," J. Opt. Soc. Am. A **9,** 1740–1748 (1992).
12. K. Freischlad and C. L. Koliopoulos, "Fourier description of digital phase-measuring interferometry," J. Opt. Soc. Am. A **7,** 542–551 (1990).
13. P. Hariharan, B. F. Oreb, and T. Eiju, "Digital phase-shifting interferometry: a simple error-compensating phase calculation algorithm," Appl. Opt. **26,** 2504–2506 (1987).
14. P. de Groot, "Phase shifting interferometer and method for surface topography measurement," U.S. patent 5,473,434 (5 December 1995).
15. The high-resolution phase-shifting mode in the Zygo Corporation MetroPro PSI software employs the 13-frame algorithm given by Eqs. (22) and (23).
16. L. L. Deck, "Phase-shifting via wavelength tuning in very large aperture interferometers," in *Optical Manufacturing and Testing III*, H. P. Stahl, ed., Proc. SPIE **3782,** 432–442 (1999).
17. P. de Groot, "Derivation of algorithms for phase-shifting interferometry using the concept of a data-sampling window," Appl. Opt. **34,** 4723–4730 (1995).
18. Y. Surrel, "Design of algorithms for phase measurements by the use of phase stepping," Appl. Opt. **35,** 51–60 (1996).